Molecular Dynamics Simulation of Liquid 2-Heptanone, Pure and Saturated with Water

Pedro Alexandrino Fernandes, M. Natália D. S. Cordeiro, and José A. N. F. Gomes*

CEQUP/Departamento Química, Faculdade de Ciências da Universidade do Porto, Rua do Campo Alegre 687, 4150 Porto, Portugal

Received: July 27, 1998; In Final Form: October 20, 1998

Molecular dynamics simulations of liquid 2-heptanone (HPT2) at 300 K were carried out using three different intermolecular potentials. The simulations were performed in two ensembles—the canonical ensemble and the isothermic−isobaric ensemble. Thermodynamic, dynamic, and structural properties were investigated. The results obtained using the three different potentials were very similar. An evaluation of the results obtained against available experimental data was performed and the most realistic potential was then chosen to simulate HPT2 saturated with water (1.41% H_2O (w/w)). Radial distribution functions were calculated and a distribution for the number of nearest neighbors was estimated. Dipole associations and other specific group associations were studied. The importance of steric factors in solvation was found to be determinant. Dynamic properties such as diffusion coefficients and orientational correlation times were estimated. It was confirmed that density plays a fundamental role in liquid dynamics. The molecular folding of HPT2 was investigated. It was found that the molecule is more tightly folded in the liquid phase than in the gas phase; as the differences are small, we obtain a picture of a liquid with mostly extended molecules. The structure and dynamics of the water molecules dissolved in HPT2 were also studied. Most water molecules form hydrogen bond-like interactions with the ketone oxygen of the HPT2 molecule, and water dynamics becomes coupled to the HPT2 dynamics. The carbonyl carbon is too hidden by *methyl* groups to solvate water oxygens. Water associations occur to a small extent. The general statistic properties of HPT2 are not affected by the presence of water, the changes being limited to the HPT2 molecules in close contact with water molecules.

I. Introduction

The study at the molecular level of liquid|liquid interfaces and of charge-transfer processes across them is fundamental to the understanding of many phenomena in chemistry, engineering, and biophysics. Ion transfer between two electrolyte solutions, phase-transfer catalysis, ion extraction, or drug delivery problems are some of such phenomena that have received much attention in the past decades.[1−6] Though much effort has been made experimentally, there are still many open questions about the exact description of the properties of the neat interfaces and the mechanism of ion transfer across them. In fact, several models with different descriptions for the ion transfer have been proposed[7−9] but their full verification was not possible, due in part to the limited knowledge of the dynamics and structure of the interfacial zone at a molecular level. There is still a debate about the correct description of the ion transfer between two immiscible liquids.[10]

Computer simulations were proven to be a fundamental tool for the elucidation of these problems. The major goal of our work is the molecular characterization of the interfacial region between water and 2-heptanone (HPT2) and the study of ion transfer between these two solvents.

HPT2 has been widely used in recent years. One of its more important applications has been precisely the ion transfer between water and organic solvents. It is immiscible with water, although the solubility of water in HPT2 (1.41% (w/w)) is not sufficiently small to be ignored. This solvent, being nonaromatic and nonhalogenated, has a very low toxicity that allows its massive use in large scale industrial ion extraction processes. (It is important to note that other solvents commonly used in liquid|liquid ion transfers, like 1,2-dichloroethane or nitrobenzene are highly toxic and their massive use seems to be environmentally unacceptable). It has been demonstrated recently that the potential range that can be applied in the system water|HPT2 plus supporting electrolytes is wide enough to perform simple and electrochemically assisted ion transfers.[11,12]

In this paper we present the results of molecular dynamics simulations of liquid HPT2, pure and saturated with water. These results should be seen as a reference state for the theoretical investigation of the interfacial region and ion transfer between water and HPT2 that is being performed in our laboratories. The possible modifications in the properties of both liquids will be detected by comparison with the pure and the saturated solvents.

This paper is organized as follows: In section II the molecular model employed as well as the details of the simulations are given. The results obtained are discussed in section III. In the last section the major conclusions of this work and its future developments are presented.

II. Computational Model

A. Molecular Model. The HPT2 molecule was represented by eight interaction sites, namely one carbonyl oxygen, one carbonyl carbon, and six united atom groups, where each carbon and their bonded hydrogens are united in one single group. Figure 1 shows a schematic representation of this molecular model. Each group is represented by a number followed by its constitution in terms of single atoms, a notation that will be frequently used in this paper.

The geometry of the water molecules corresponds to that given by the SPC/E model.[13]

10.1021/jp983170v CCC: $18.00
Published on Web 02/03/1999

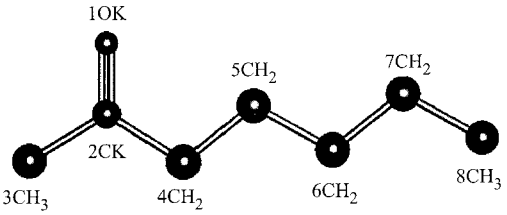

Figure 1. Molecular model of HPT2. Each site has a corresponding label.

TABLE 1: Point Charge Distributions for HPT2

$1O_k$	$2C_k$	$3CH_3$	$4CH_2$	$5CH_2$	$6CH_2$	$7CH_2$	$8CH_3$
−0.540	0.517	0.016	−0.037	0.043	−0.005	0.021	−0.015

B. Potentials. *1. Intramolecular Potential*. The water molecules were considered to be rigid. This procedure allows us to increase the time step used to 1.0 fs, which allows better exploration of the configurational space, has no influence in the results obtained, as previously checked, and may be justified by the absence of coupling between water stretching and bending and other vibrations in our system.

Flexible bonds, angles, and dihedrals were included in the intramolecular potential of HPT2. In addition, one improper dihedral was used in order to keep the planarity of the sp2 carbon. All potential parameters were taken form the CHARMm force field[14] and are given by the following expression, with obvious notations:

$$V = \sum^{\text{bonds}} K_{ij}(r_{ij} - r_{ij}^{\text{eq}})^2 + \sum^{\text{angles}} K_\theta(\theta - \theta^{\text{eq}})^2 + K_{\text{impr}}(\theta_{\text{impr}} - \theta_{\text{impr}}^{\text{eq}})^2 + \sum^{\text{dihedrals}} K_{\text{dih}}(1 + \cos(m\theta_{\text{dih}} - \delta)) \quad (1)$$

One to four specific dihedral interactions were included, as established in the CHARMm force field.

2. Intermolecular Potential. The intermolecular potential (pairwise additive) was represented by the sum of one Coulombic potential with one Lennard-Jones potential

$$V_{ij} = \frac{q_i q_j}{r_{ij}} + 4\epsilon_{ij}\left(\left(\frac{\sigma_{ij}}{rij}\right)^{12} - \left(\frac{\sigma_{ij}}{r_{ij}}\right)^{6}\right) \quad (2)$$

More complex interaction potentials would make two-phase simulations impracticable with current computational resources.

The transferability of intermolecular potential parameters has been extensively discussed in the past decades. In fact, a transferable force field will largely expand the usefulness of computer simulations. Several attempts have been made, but the reliability of those force fields is far from perfect, although some progress has been achieved. It is especially important to evaluate the ability of the force fields in the modeling of liquids not used in their parametrization.

In this work we tested the Lennard-Jones interaction potential parameters of the OPLS[15] and CHARMm[14] force fields.

The electrostatic potential was determined by quantum calculations at the Hartree−Fock level, with the 6-31G** basis set, using the program Gaussian94.[16] The molecular electrostatic potential distribution obtained has been fitted to point charges, condensing hydrogens into heavy atoms, using the restrained ESP fit method.[17] The set of point charges obtained is presented in Table 1, and will be called charge group I (CGI).

When using OPLS Lennard-Jones parameters, we also checked the results obtained not only with the point charges described above but also with the proper OPLS electrostatic charges for ketones (charge group II, CGII).

Three intermolecular potentials could thus be defined and were tested on the simulations of pure HPT2, namely OPLS+CGI (OPLS-I), OPLS+CGII (OPLS-II) and CHARMm+CGI (CHARMm-I). The thermodynamic, dynamic, and structural results of pure HPT2 obtained using these intermolecular potentials were all very similar. The OPLS-I potential was chosen to simulate hydrated HPT2.

For water, the SPC/E model[13] was used, as it includes effective polarization and was proven to give reliable results in condensed phases.

The potential parameters for the interactions between HPT2 and water were calculated using the standard rules $\sigma_{ij} = {}^1/_2\,(\sigma_i + \sigma_j)$ and $\epsilon_{ij} = (\epsilon_i\epsilon_j)^{1/2}$. This procedure is consistent with the usual rules used in the statistical mechanics of mixtures and with the independent determination of the H_2O-H_2O and HPT2−HPT2 potentials. However, these combination rules are only an approximation and a fit of the parameters to quantum calculations of the dimer H_2O−HPT2 and to the thermodynamical properties of H_2O/HPT2 solutions would be desirable.

C. Method. All molecular dynamics simulations were performed with the DL_POLY program.[18] These simulations have been carried out in two ensembles: the canonical ensemble and the isothermic−isobaric ensemble. In both ensembles a Nosé−Hoover thermostat[19] has been used. In the isothermic−isobaric ensemble a Nosé−Hoover barostat[20] has been also employed to maintain the pressure at 1 bar.

Periodic boundary conditions were used in all three directions. The Ewald summation method with tinfoil boundary conditions was used to deal with Coulombic forces. A spherical molecular cutoff (11 Å) for the real space part of the Ewald energy as well as for the short-range potentials was applied.

The integration of the equations of motion was performed with a time step of 1 fs. A multiple time step algorithm[21] was implemented with an actualization frequency of 10 fs. This algorithm was only used for interactions at a distance larger than 9 Å. It was previously verified that this procedure led to good energy conservation (without thermostat) and did not affect the energetic and dynamic behavior of the systems.

1. Pure HPT2 Simulations. The system was modeled by 234 molecules of HPT2 confined to a rectangular box with initial dimensions of 34.64 Å × 34.64 Å × 45.52 Å. The cell size was chosen in order to reproduce the experimental liquid density (0.8124 g/cm^3).

The three HPT2 systems, obtained by the use of the three different intermolecular potentials, were equilibrated in a simulation of 300 ps in the *NVT* ensemble. All energetic terms, temperature, and pressure were stabilized and seen to be oscillating around their mean values. It was concluded that the systems reached equilibrium.

Starting from the final configurations of the equilibration runs, three independent simulations in the same ensemble were performed each with 300 ps length, from where the results presented here were taken.

Simulations in the *NPT* ensemble were also performed, one with each of the intermolecular potentials, starting from the equilibrated configurations obtained in the previous simulations. Further equilibration during 150 ps was necessary to achieve equilibrium in this new ensemble, after which three simulations of 300 ps each were made for data collection.

2. Simulations of HPT2 Saturated with Water. The simulated system consisted of a mixture of 232 HPT2 molecules and 21 water molecules, to obtain the experimental solubility of water in HPT2. The water molecules were randomly inserted in a 34.64 Å × 34.64 Å × 45.78 Å simulation cell previously filled

with equilibrated HPT2. Then the HPT2−H_2O and H_2O−H_2O interactions were slowly increased from zero to their final values. We considered additive volumes to choose the initial cell volume, which was only a starting point from which an equilibration of 200 ps in the *NPT* ensemble was performed.

After equilibration, all energetic terms, temperature, volume, and pressure were stabilized and oscillating around their mean values, this meaning that the systems reached equilibrium. Starting from the last configuration obtained, a simulation of 1200 ps was performed in the *NPT* ensemble for data collection, from where the results were taken.

III. Results

The results of the simulations are now presented. These results can be seen not only as a study of liquid HPT2, pure and hydrated, but also as a reference state, which shall be used for comparison with the properties of interfacial HPT2 in the biphasic system water|HPT2, which is currently under investigation in our laboratories.

All errors associated with numerical quantities presented in this paper correspond to twice the standard deviation of the mean of the related quantities.

A. Thermodynamics. Some of the usual thermodynamic quantities, like the density (*NPT* ensemble) and the heat of vaporization (*NVT* and *NPT* ensembles) have been calculated. These two properties are the usual targets in the optimization of potentials for liquid simulations and were extensively used in the establishment of general transferable force fields. So, it is especially interesting to check the accuracy of the present force fields in reproducing these thermodynamic properties in a complex liquid like HPT2, which was not used in the establishment and optimization of the force field parameters.

The density has only been computed in the *NPT* ensemble as in the *NVT* ensemble it is fixed by the choice of the cell size.

The enthalpy of vaporization (ΔH_v) at 300 K was estimated according to eq 3

$$\Delta H_v = E_{dih}(g) + E_{intra}^{1-n,n>4}(g) - (E_{dih}(l) + E_{intra}^{1-n,n>4}(l) + E_{inter}(l)) + RT \quad (3)$$

where E_{dih} represents the dihedrals energy (including 1−4 interactions), E_{inter} is the intermolecular energy and $E_{intra}^{1-n,n>4}$, are the interactions between groups of the same molecule separated by more than three bonds.

The change in internal energy for the liquid−gas transition can be separated into kinetic, intermolecular, and intramolecular terms. In an ideal gas approach the change in intermolecular energy for the liquid → gas transition corresponds to the symmetric gas of the liquid's intermolecular energy since the molecules do not interact with each other. Concerning the kinetic and intramolecular energy, we adopted the widely used Jorgensen's approach,[22] which considers that the sum of the vibrational terms plus the kinetic energy is equal in gas and liquid phases. Thus these terms cancel each other and vanish from eq 3. The missing terms in the intramolecular energy are then the dihedral energy (which is obviously different in liquid and gas) and the interaction energy between groups inside the same molecule separated for more than three bonds.

For comparison, the value of the intermolecular energy decomposed in their Coulombic and Lennard-Jones terms was also computed. All these results are presented in Table 2.

The densities obtained using the three potentials agree quite well with the experimental results. The density is slightly overestimated with all potentials, by 3.5% using the OPLS-I potential, by 3.6% using the OPLS-II potential, and by 4.6% using the CHARMm-I potential.

TABLE 2: Thermodynamic Results for Pure HPT2 (Energies in kJ/mol; Densities in g/cm^3)

	CHARMm-I	OPLS-I	OPLS-II
		NVT	
ΔH_v	49.00 ± 0.01	47.26 ± 0.01	45.90 ± 0.01
en elect	−6.19 ± 0.01	−5.52 ± 0.01	−4.85 ± 0.01
en VdW	−46.26 ± 0.01	−47.41 ± 0.01	−47.40 ± 0.01
		NPT	
density	0.850 ± 1 × 10^{-4}	0.8450 ± 1 × 10^{-4}	0.8415 ± 1 × 10^{-4}
ΔH_v	51.27 ± 0.01	49.05 ± 0.01	47.52 ± 0.01
en elect	−6.49 ± 0.01	−5.70 ± 0.01	−5.02 ± 0.01
en VdW	−48.33 ± 0.01	−48.93 ± 0.01	−48.95 ± 0.01

For HPT2 there are two boiling points measured at normal pressure reported in the literature.[23] The value of 52.21 kJ·mol^{-1} [23] was measured for the heat of vaporization of HPT2 at the boiling point. The heat of vaporization at 300 K was estimated to be 56.90 and 58.16 kJ·mol^{-1} for the two boiling points available.

The enthalpy of vaporization is underestimated by all three potentials. The relative differences in the calculated and experimental heats of vaporization shown below were estimated by considering both experimental heats of vaporization. The one corresponding to the 58.16 kJ·mol^{-1} value is always presented inside parentheses.

In the *NPT* ensemble the differences to the experimental values are −16.5% (−18.3%) using the OPLS-II potential, −13.8% (−15.7%) using the OPLS-I potential, and −9.9% (−11.8%) using the CHARMm-I potential. The values of the enthalpy of vaporization computed for the *NPT* ensemble are slightly better than the ones of the *NVT* ensemble.

Although not so precise as the density, the enthalpy of vaporization obtained seems very reasonable for a property calculated using general transferable force fields that did not include HPT2 in their parameters optimization process.

It is also important to note the similarity in the van der Waals energy obtained using the three different intermolecular potentials. As the general dynamics of this liquid is mainly controlled by dispersive forces, analogous results are obtained for the structure and dynamics of HPT2 when employing those potentials, as will be seen in this paper.

Thus it can be concluded that, when nonelectrostatic interactions are dominant, transferable force fields can give a reasonable estimation of the thermodynamic properties discussed here, even in the case of highly complex liquids such as HPT2.

The OPLS-I potential seems to be the more realistic potential, as it presents a slightly better compromise between density and heat of vaporization, and simulations of hydrated HPT2 were performed with that potential.

Here, it is interesting to note that the density obtained for hydrated HPT2 [(0.8380 ± 2) × 10^{-4} g/cm^3] is smaller than the density of pure HPT2 [(0.8405 ± 2) × 10^{-4} g/cm^3], estimated with the same potential. An explanation for this observation is discussed below.

B. Structure. *1. Molecular Folding*. To estimate the extent of molecular folding, we could analyze the dihedral angle populations. This procedure would be helpful if applied to molecules with one or two dihedral angles, but in the case of HPT2 with five dihedral angles it seems inappropriate. As our objective was to estimate the variety and frequency of the conformations that the molecule, as a whole, might present, the individual dihedral populations are not very illustrative.

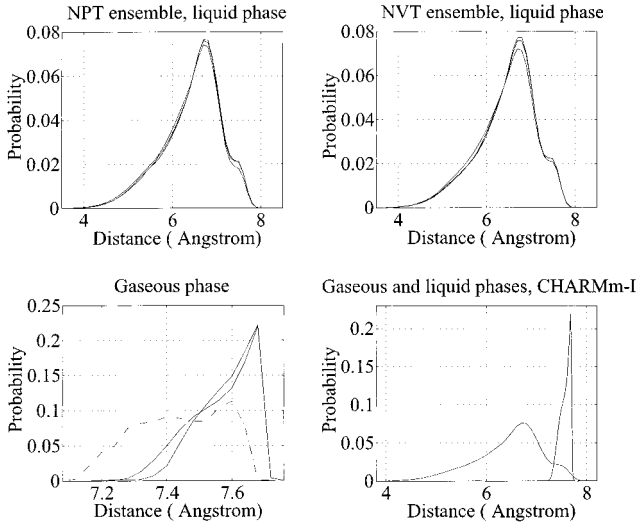

Figure 2. Probability distribution of the distances between the $3CH_3$ and the $8CH_3$ groups. The four graphics represent those distributions in the *NPT* ensemble, *NVT* ensemble, and in the gas phase (where the dashed line corresponds to OPLS-II potential), and the comparison between the results in the gas phase and the liquid phase for CHARMm-I potential in the *NPT* ensemble. When the results are almost equivalent, no explicit distinction is made between the corresponding potentials.

TABLE 3: Molecular Folding of HPT2 (All Values in Å)

	CHARMm-I	OPLS-I	OPLS-II	OPLS-I(sat)
		NPT		
maximum	6.7	6.7	6.7	6.7
plateau	7.3−7.5	7.3−7.5	7.3−7.5	7.3−7.5
mean	6.45	6.46	6.42	6.47
		NVT		
maximum	6.8	6.6	6.7	
plateau	7.3−7.5	7.3−7.5	7.3−7.5	
mean	6.47	6.48	6.44	

Our option was the calculation of the distribution of the distance between the groups $3CH_3$ and $8CH_3$. These distributions have been calculated for all simulations in the liquid phase. Simulations of a single monomer were performed with each potential in order to estimate the same distributions in the gas phase. The distributions obtained are depicted in Figure 2. In Table 3 we present numerical details related to Figure 2.

The distance between the $3CH_3$ and $8CH_3$ groups in the conformation of Figure 1 (7.675 Å) can be taken as a reference. In that conformation all bonds and angles take their equilibrium value and all dihedrals (with the exception of the $1O_k-2C_k-4CH_2-5CH_2$ one) are in the trans conformation.

It can be seen that the molecular folding and the variety of significantly populated conformations is higher in the liquid phase than in the gas phase. This result should be expected as intermolecular interactions in the gas phase are negligible and, thus, the monomers tend to adopt the conformations that have minimal intramolecular energy, with thermal fluctuations around it.

In the liquid phase, the strong interactions with neighbors induce the adoption of conformations that minimize the total energy of the molecule (intramolecular plus intermolecular). As there is a wide distribution of neighbors, the minimal energy conformations are more broadly distributed in molecular length space. For the HPT2 molecule the minimum of total energy depends not only on the intramolecular energy but also on intermolecular terms and may be achieved for conformations that do not correspond to the minimal internal energy, as is clear by close inspection of Figure 2.

The larger density of the liquid phase reduces the average volume accessible to each molecule, which also contributes to the decrease of the molecular length.

It is interesting to observe the existence of a plateau in the molecular size distribution which extends from 7.3 to 7.5 Å. The molecules with that length seem to show additional stability, by the fact that the decrease in population with increasing length is strongly attenuated. The phenomenon can be understood as a strong decrease in dihedral energy (which is very close to the absolute minimum, as can be seen in the gas phase distributions) that is not compensated by an equally strong increase in the intermolecular energy, less sensitive to so small variations of the molecular length.

The similarity of the results for the liquid-phase molecular folding that are obtained with the three potentials is obvious. The simulations in the *NVT* ensemble present a mean length a little bit higher than the one obtained in the simulations in the *NPT* ensemble, a fact clearly related to the increased density of this last ensemble. In all cases, the difference corresponds to 0.02 Å. The presence of water in saturated HPT2 does not affect significantly the average degree of folding of the HPT2 molecules, and the probability distribution for the molecular folding of saturated HPT2 is seen to be indistinguishable, within statistical uncertainty, from that of the pure HPT2 for the same potential.

2. Structure of the HPT2 Solvation Shell. a. Global Structure of the Solvation Shell. Due to the large molecular size and heterogeneity of groups in the molecule, it is expected that the solvation between HPT2 molecules will strongly depend on the type of site and on the position of the site in the molecule. It is obvious that oxygen solvation is different from *methyl* solvation. For similar groups, their solvation will be different if one compares a peripherical group with a central group. So, the global structure of the solvation shell cannot be analyzed by observing the individual solvation of the eight different groups of the molecule. It is important to begin considering the molecule as a whole in order to evaluate its global solvation details, like the dimension of the global solvation shell and the distribution of the number of neighbors inside it.

To this end, each molecule was condensed into its center of mass (com) and the com radial distribution functions were computed.

Radial distribution functions (RDF) exhibit the differences on the distributions of a particle around a predefined center in relation to a structureless homogeneous distribution at macroscopic density.

The density of particles y around a particle x is given by

$$\rho_{y(x)}(r) = \rho^{\circ}_{y(x)}\, g_{y(x)}(r) \tag{4}$$

where $\rho^{\circ}_{y(x)} = (N_y/V)$ is the average number density of y particles, $\rho_{y(x)}(r)$ is the number density of particles y at a distance r of particle x, and $g_{y(x)}(r)$ is the RDF of the y particle around x.

Considering $y = x =$ com, we obtain a density profile as a function of the distance from the com of each molecule. This RDF illustrates the mass aggregation of the liquid without considering the details of specific associations between groups of the molecule, which will be discussed in the next section. Figure 3 depicts the RDFs obtained. In hydrated HPT2 we also estimated the O_w-com RDF, where O_w refers to the water oxygen. This gives us a picture of the mass aggregation around water molecules.

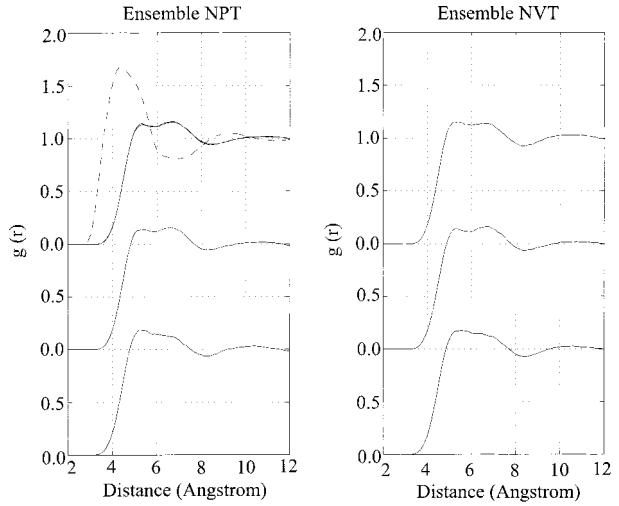

Figure 3. The com radial distribution functions in the *NPT* (left) and in the *NVT* (right) ensembles. Each graphic depicts the com RDFs calculated using, respectively, from top to bottom, the OPLS-I, OPLS-II, and CHARMm-I potentials. The three lines in the top left graphic represent the com RDFs for pure and hydrated HPT2 (solid lines, almost coincident) and the O_w-com RDF (dashed line).

The distributions obtained using the three potentials are very similar. They present a broad peak at ca. 5−7 Å, where the density is about 15% higher than its average value. The peak is not very high due to its broadness. The position of the first minimum of the RDF can be considered as the radius of the first solvation shell. It is located at 8.3 Å in all simulations in the *NPT* ensemble and at 8.4 Å in all simulations in the *NVT* ensemble (a little more distant due to the lower density). So, a first solvation shell for HPT2 appears with a radius up to 8.3−8.4 Å. The massic aggregation of HPT2 is not significantly affected by the dissolved water, and the RDFs for pure and hydrated HPT2 are almost coincident.

In the top left RDF of Figure 3 we also show the O_w−com RDF (dashed line). A clearly defined peak centered at 4.4 Å is seen and, upon integration, it may be shown to contain an average of 6.4 HPT2 molecules near the water molecule. This solvation of water by HPT2 will be studied in more detail in the next section.

The distribution of the number of neighbors inside the HPT2 first solvation shell is presented in Figure 4.

As can be seen, the results are almost independent of the potential or ensemble considered. The diversity in the number of neighbors that a monomer can have illustrates the variety of environments the molecules are submitted to. A number of neighbors between eight and twelve is the more frequent situation (93% of the cases, independently of the potential or ensemble), ten being the most likely number.

The average number of neighbors was also calculated and is given in the figure caption. It is also almost independent of the potential or ensemble.

b. Detailed Structure of the Solvation Shell. For a molecule with eight different sites, 36 different RDFs can be defined. Although we analyzed many of the RDFs of the liquid, it seems that it would be redundant to show all of them here, so we selected the ones that seemed more important for the description of the structure of the liquid.

b.1. RDF for the $1O_k$ −$2C_k$ Sites. This RDF allows us to evaluate the associations induced by the polar part of the molecule. Figure 5 illustrates the results obtained.

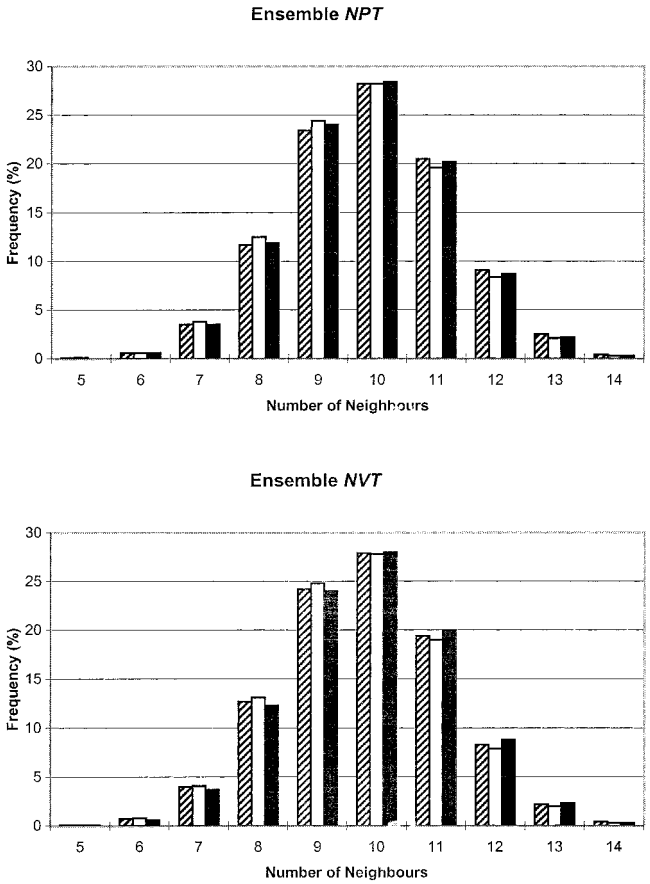

Figure 4. Distribution of the number of neighbors for the RDFs of the com of HPT2. The dashed bar corresponds to the CHARMm-I potential, the white bar corresponds to the OPLS-I potential, and the solid bar corresponds to the OPLS-II potential. In the *NPT* ensemble (top) the average number of neighbors was found to be 9.9, 9.8, and 9.8 using the CHARMm-I, OPLS-I, and OPLS-II potentials, respectively. In the *NVT* ensemble (bottom), an average of 9.8 neighbors was obtained independently of the potential.

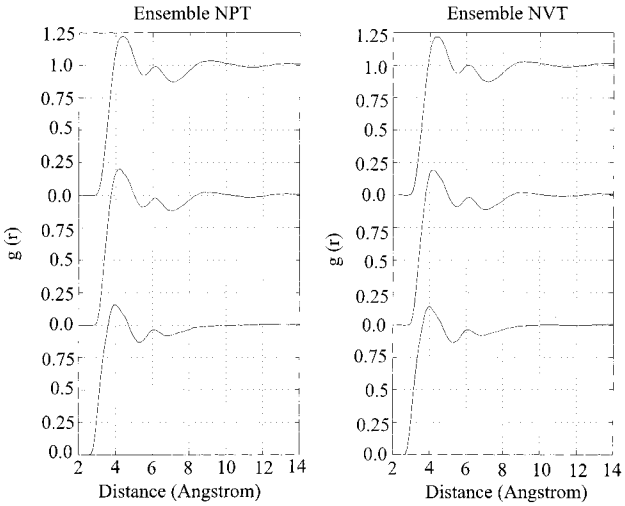

Figure 5. RDFs for the $1O_k$−$2C_k$ atoms. The three RDFs in each graphic correspond, from top to bottom, to the OPLS-II, OPLS-I, and CHARMm-I potentials.

Although there is a small difference in the depth of the second minimum, the results obtained using the three potentials are quite similar.

Charge distribution CGI attributes greater charge to the groups considered here and causes a stronger association between those groups. This can be seen by the closest location of the first

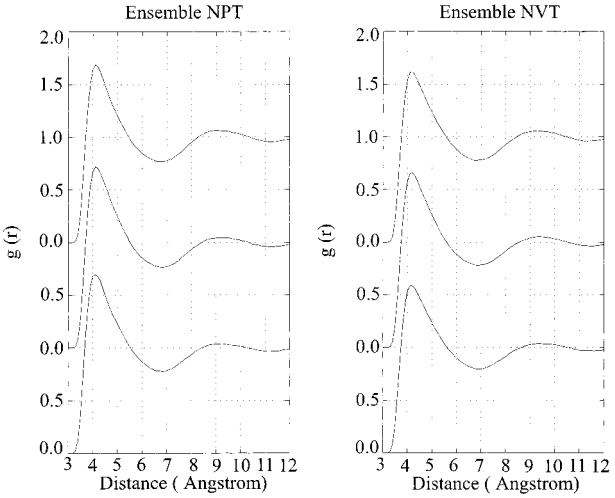

Figure 6. RDFs for the terminal group $8CH_3$. The three RDFs in each graphic correspond, from top to bottom, to the OPLS-II, OPLS-I, and CHARMm-I potentials.

peak when using CGI (4.2 Å using the OPLS-I potential and 4.4 Å using the OPLS-II potential, in both ensembles). Integration of the first peaks allows us to estimate an average number of neighbors of 2.6, 2.6, and 2.4 for the *NPT* ensemble and 2.5, 2.5, and 2.2 for the *NVT* ensemble. These values correspond to the OPLS-II, OPLS-I, and CHARMm-I potentials, respectively.

The relatively long distance at which the maxima of the first peaks are centered reflects the stereochemical difficulty of the approach to the carbonyl carbon, due to the presence of the *methyl* groups of the carbonated chain. This stereochemical barrier reduces the intensity and the importance of dipole associations.

b.2. RDF for the $8CH_3-8CH_3$ Sites. This RDF is especially relevant to show the importance of steric factors in the solvation of HPT2. In fact, it is between terminal groups that solvation becomes more well-defined. As can be seen in Figure 6, this RDF has the highest first peak of all RDFs already shown.

Such a well-defined solvation shell is not the result of any specificity of the $8CH_3-8CH_3$ interaction, which is very similar to the other interactions between groups of the carbonated chain (as $4CH_2-5CH_2$) but is due to the stereochemical facility in accessing terminal groups. This behavior is also observed in the $3CH_3-8CH_3$ RDF (not shown here) but in a minor scale, because that association does not allow for dipole associations.

Integration of the first peaks allows us to estimate an average number of neighbors of 4.1, 4.1, and 4.1 for the *NPT* ensemble and 4.2, 4.2, and 4.1 for the *NVT* ensemble. These values correspond to the OPLS-II, OPLS-I, and CHARMm-I potentials, respectively.

3. H_2O-H_2 O and HPT2$-H_2O$ Pair Correlations. As observed in the last sections, the average effect of water in the HPT2 properties is almost negligible. A statistical characterization of HPT2 properties hides the influence of the small amount of water in the mixture. However, near an interface between water and HPT2 the composition of the system can be much richer in water. So, it is important to analyze the water−HPT2 pair correlations to have a reference state from which the possible structural changes of HPT2 near an aqueous interface may be detected. In this section H_2O-H_2O and H_2O−HPT2 RDF are presented and the most common structures involving water are discussed.

a. Water Pair Correlation Functions. Figure 7 presents the oxygen−oxygen (O_w-O_w) and the oxygen−hydrogen (O_w-H_w) RDFs. The peaks are slightly displaced toward larger

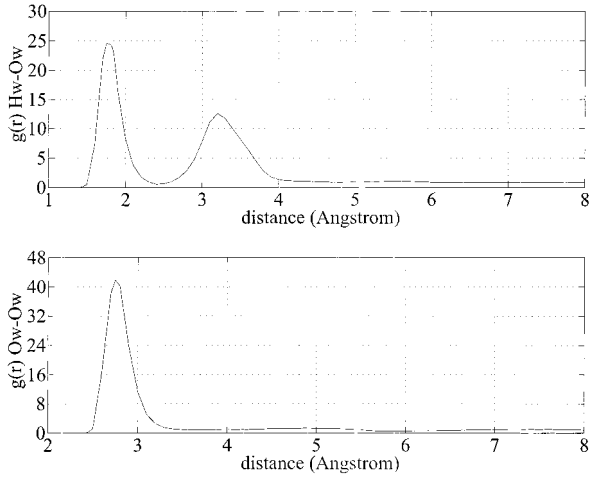

Figure 7. RDFs for the H_w-O_w (top) and the O_w-O_w (bottom) atoms in saturated HPT2.

distances (+0.2 Å) when compared to the same RDFs in pure water. In the H_w-O_w RDF, the height of the second peak is about one-half of the height of the first peak (in pure water they have almost the same height), reflecting the depletion of the second coordination shell of water. Integration of the H_w-O_w RDF first peak leads to an estimate of the number of neighbors in the first coordination shell and results in a value of 0.19 oxygens per water hydrogen. Notice that, if all water hydrogens form a hydrogen bond with a water oxygen, and considering that the same hydrogen cannot make more than one hydrogen bond, we would obtain upon integration of the first peak of the H_w-O_w RDF an average number of neighbors of 1. As we have obtained a number of 0.19, this means that only 19% of the hydrogens do form hydrogen bonds with the water oxygen.

In pure water we obtain an average of 0.94 oxygens per water hydrogen. This gives a picture of water molecules with a solvation shell geometry resembling that obtained for pure water, although incomplete due to the reduced water density.

The average coordination number of water in saturated HPT2 can be obtained by integration of the O_w-O_w first peak. We obtained an estimate of 0.83 neighbors. In independent simulations of pure SPC/E water, we obtained an average coordination number of 5.4 neighbors.

If we compare the coordination numbers of water in pure and in saturated HPT2 in relation to the density of water in these two environments it becomes clear how resistant is the structure of water. Changing from pure water to saturated HPT2 decreases the density of water by 78 times but its coordination number only decreases 6.5 times. It is very important to consider the robustness of the water structure to changes induced by the presence of HPT2 to correctly understand the structure of the liquid−liquid interface between these two solvents.

b. Water−HPT2 Pair Correlations. After analyzing several pair correlation functions between water and HPT2 it was found that the only well-defined (and energetically more favorable) pair correlation was the one formed between the water hydrogen and the ketone oxygen.

The H_w-1O_k RDF is presented in Figure 8. A very well-defined peak, located at the same distance as the first peak of the H_w-O_w RDF, gives under integration an average of 0.72 neighbors; this reveals that an average of 72% of the water hydrogens form a hydrogen bond with the ketone oxygen. An energy criterion frequently used to define a hydrogen bond (E_{Hb} $\leftarrow$ 2.4 kcal·mol^{-1}) would not consider most of those interactions

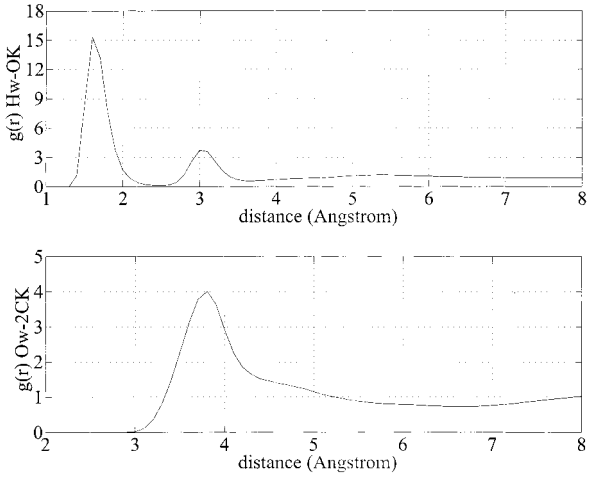

Figure 8. RDFs for the H_w-1O_k (top) and the O_w-2C_k (bottom) atoms in saturated HPT2.

as hydrogen bonds, as its interaction energy tends to be slightly higher than the traditionally accepted limit, although a distance criteria would consider as hydrogen bonds most of the H_w-1O_k interactions. More than the exact definition of a hydrogen bond, the designation used in this paper aims at making it easier to understand the water−HPT2 pair correlations.

In Figure 8 we can also see the O_w-2C_k RDF. It becomes clear that the water oxygen is not solvated by the carbonyl carbon. The first peak is centered at 3.8 Å and is caused by the H_w-1O_k hydrogen bridges, which induce the approximation between the carbonyl carbon and the water oxygen. The *methyl* groups bonded to the carbonyl carbon form a stereochemical barrier to the water oxygen.

At this point it is also interesting to estimate the most probable hydrogen bond angle. Considering the oxygen−hydrogen bond length (1.0 Å) and the location of the first peaks of the H_w-1O_k RDF (1.8 Å) and of the O_w-1O_k RDF (2.8 Å), we conclude that the most probable $O_w-H_w-O_k$ angle is 180°, indicating a linear hydrogen bonding.

c. Solvation Sphere of Water in Saturated HPT2. It becomes important here to draw a picture of the coordination sphere of water. We considered independent interactions with the water oxygen and water hydrogen. From the RDFs analyzed so far, we already know that the only energetically significant interaction with the water oxygen corresponds to the hydrogen bridges established with hydrogens of other water molecules. Integration of the first peak in the H_w-O_w RDF allows us to conclude that 81% of the possible hydrogen bonds with the water oxygens are not established while 19% are solvated by water hydrogens.

To get a more complete picture of the near water environment, a similar procedure was used to investigate the most important interactions of hydrogen. A water oxygen at a distance to another water hydrogen smaller than the first minimum in the H_w-O_w RDF was considered to be hydrogen bonded to the water hydrogen. Similarly, a ketone oxygen closer to a hydrogen than the distance of the first minimum of the H_w-1O_k RDF was also considered to be hydrogen bonded to that hydrogen. From integration of the first peaks in the H_w-O_w and H_w-Ok RDFs we can conclude that 19% of the hydrogens form hydrogen bonds with water oxygens, 72% of the hydrogens form hydrogen bonds with ketone oxygens, and 9% of the hydrogens do not establish any significant interaction.

We get a picture of water molecules where hydrogens are mainly interacting with ketone oxygens via hydrogen bonds, although water associations are not negligible, and most water oxygens do not establish any significant interaction.

Thus, the most common structure of the water coordination sphere corresponds to a water molecule where the oxygen is not solvated and is making two hydrogen bonds with two HPT2 molecules. This results in a very large radius of solvation, and is one of the factors that can justify the decrease in density of saturated HPT2 when compared to pure HPT2.

C. Dynamics. In this section we report the results of the study of the dynamic properties of HPT2 and water. Diffusion coefficients and orientational correlation times were computed. All results are presented in Figures 4 and 5. The density of all systems is also presented.

1. Diffusion Coefficients. The diffusion coefficients for the com of HPT2 have been calculated according to the relation of Einstein:

$$D = \lim_{t\to\infty} \frac{\Delta R^2}{6t} \tag{5}$$

where D is the diffusion coefficient, ΔR is the com displacement, and t is the time. Each simulation of pure HPT2 was divided in 10 blocks of 30 ps each. The simulation of the saturated HPT2 was divided in 40 blocks of 30 ps each. The diffusion coefficients have been computed in each block. In Figures 4 and 5 we present the mean value of the diffusion coefficients and the respective errors.

Density plays a fundamental role in the dynamic properties of liquids. In diffusion the displacement of a particle is limited by the interactions with neighbors. An increase in density causes a decrease in the mean free path accessible to each particle and the meantime displacement tends to decrease.

Comparing the results obtained in the *NVT* ensemble, we see that they are very similar. This might be expected by the fact that all simulated systems in this ensemble have the same density.

In the *NPT* ensemble the results obtained, although very similar, vary according to the density. The correct order for this variation is obtained. Increasing the density always leads to a decrease in the diffusion coefficients.

Comparing the results obtained in the two ensembles, we note that the same order of variation of the diffusion coefficients with density is obtained. The diffusion coefficients obtained in the *NVT* ensemble, where the density is lower, are always higher than the ones obtained with the same potential in the *NPT* ensemble.

It can be said that all diffusion coefficients obtained lie in the range of 1.0×10^{-9} to 1.5×10^{-9} $m^2\ s^{-1}$ and they have a strong dependence on the density.

As density is determinant, the diffusion coefficients estimated in the *NVT* ensemble should be considered the most reliable, but this cannot be confirmed by the lack of experimental data. Water molecules in saturated HPT2 present diffusion coefficients quite close to HPT2. The water molecules are strongly coupled to HTP2 via hydrogen bond interactions, and both molecules tend to move together.

D. Orientational Correlation Times. The normalized vector $\vec{v} = \overrightarrow{3CH_37CH_2}$ has been considered as representative of the orientation of the HPT2 molecules. The normalized time autocorrelation function for this vector has been calculated according to the following equation:

$$C(\xi) = \langle v(t)\ \vec{v}(\xi + t)\rangle_t\ C(0)^{-1} \tag{6}$$

where the brackets represent a mean over all time origins t.

TABLE 4: Dynamic Results for Pure HPT2 (All Diffusion Coefficients in $m^2 s^{-1}$; Orientational Correlation Times in ps)

	CHARMm-I	OPLS-I	OPLS-II
	NVT		
10^9D	1.5 ± 0.1	1.4 ± 0.1	1.5 ± 0.1
t_{corr}	27 ± 1	29 ± 1	27 ± 1
	NPT		
10^9D	1.0 ± 0.1	1.2 ± 0.1	1.1 ± 0.1
t_{corr}	38 ± 2	33 ± 1	34 ± 2
density	0.8501	0.8405	0.8415

TABLE 5: Dynamic Results for Hydrated HPT2 (All Diffusion Coefficients in $m^2 s^{-1}$; Orientational Correlation Times in ps)

	OPLS-I (HPT2)	SPC/E (water)
	NPT	
10^9D	1.36 ± 0.06	1.4 ± 0.1
t_{corr}	30 ± 1	30 ± 1 (HH), 24 ± 1 ($\vec{\mu}$)
density	0.8380	0.8380

The autocorrelation time for the orientation of the molecule was also computed as

$$t_{corr} = \int_{\xi=0}^{\infty} C(\xi)\, d\xi \qquad (7)$$

These autocorrelation times have been estimated in all simulations and are presented in Figures 4 and 5. In saturated HPT2 the water reorientation was also studied, but in this case, the time autocorrelation function for the $\overrightarrow{HH}$ and for the dipole moment vectors of the water molecules were estimated.

Because of the very slow decay of the correlation function and due to block analysis, this function has only been computed until 20 ps, and an exponential fit was made to estimate the value of the integral in eq 7 from 20 ps till infinity. This procedure has been tested by comparing the results of the extrapolations with one estimation of the correlation function up to 200 ps using all data produced in the entire simulation, and it seems to be very accurate.

Analyzing Figures 4 and 5, we can draw the same conclusions from the orientational correlation times as from the analysis of the diffusion coefficients. Once again, the results obtained in the *NVT* ensemble with the three potentials (where the density is the same) are very similar, and the results obtained in the *NPT* ensemble, although very close, follow the density variations. In all cases, the correct order for the variation of the autocorrelation time with density is obtained. Increasing the density always leads to an increase in the autocorrelation times. This can be seen by comparing the three results obtained in the *NPT* ensemble and also comparing the results obtained with the same potential in both ensembles.

From Table 5, we may conclude that the orientational dynamics of water becomes closely related to the HPT2 dynamics. As the water molecules are hydrogen-bonded to the HTP2 molecules, and one water molecule has not more than two neighbors in conditions to form hydrogen bonds (contrarily to bulk water), they cannot rotate independently without destroying their hydrogen bonds.

IV. Conclusions

The study presented here shows the capacity of molecular dynamics simulations to produce detailed structural and dynamic information, at a molecular scale, in a complex organic liquid such as 2-heptanone.

The similarity of the results obtained using two different force fields confirms the reliability of the transferability of the potentials, which is known to be especially favorable in systems where Coulombic interactions do not assume a fundamental role in the system dynamics.

In this work thermodynamic quantities such as density and enthalpy of vaporization have been computed, and agreement was found with experimental data.

The diffusion coefficients and orientational correlation times have been estimated. It was observed that water translational motion becomes coupled, via H_w-1O_k hydrogen bonds, to the HPT2 motion.

The dependence between dynamic properties and density was analyzed and discussed. It was concluded that the dynamics of the system is strongly accelerated with the decrease of the density.

The extent of molecular folding has been investigated showing that the molecules are mostly extended, although not so much as in the gas phase. The presence of water does not significantly influence the HPT2 folding.

The HPT2 solvation sphere has a radius of 8.3−8.4 Å and contains around eight to twelve neighbors inside it, ten being the most likely number. The solvation of specific groups was not found to be very relevant. Steric factors do not allow strong associations except in the case of terminal groups.

Water molecules are mainly solvated through the H_w-1O_k interactions (72% of the cases in average). Water−water hydrogen bonds still exist, but less frequently (19% of the hydrogens participate in hydrogen bonds with water oxygens). Water oxygens are mainly unsolvated, although a small number (19%) form hydrogen bonds.

Traditionally, the intermolecular potential optimizations are performed in order to reproduce the density and enthalpy of vaporization of the real liquid. In our study, which was not concerned with direct energetic measurements, it has been verified that density has a visible influence in the results obtained, especially in the dynamic results. However, the differences in the entalphies of vaporization obtained with the three potentials did not have any well-defined influence in the results. It seems that structural and dynamic properties are not very sensitive to variations in the enthalpy of vaporization.

The shape and size of the molecule has a strong influence on the structure and dynamics of the liquid and is independent of the intermolecular potential used.

In a study whose goals are mainly the dynamic and structural properties, it should be emphasized that the optimization of the enthalpy of vaporization, although important, can eventually be not so fruitful as the optimization of the structural parameters.

Acknowledgment. Financial support from Fundação para a Ciência e a Tecnologia (Lisbon) through project PRAXIS/PCEX/QUI/61/96 is acknowledged. P.A.F. thanks the Programa Praxis XXI for a doctoral scholarship (BD/9175/96). Helpful discussions with Prof. A. Fernando Silva of this department are gratefully acknowledged.

References and Notes

(1) *Faraday Discuss. Chem. Soc.* **1984**, *77*, .

(2) Honing, B. H.; Hubbell, W. L.; Flewwlling, R. F. *An. Rev. Biophys., Biophys. Chem.* **1986**, *15*, 163.

(3) *The Interface Structure and Electrochemical Processes at the Boundary Between two Immiscible Liquids*; Kazarinov, V. E., Ed.; Springer: Berlin, 1987.

(4) Arai, K.; Ohsawa, M.; Kusu, F.; Takamura, K. *Bioelectrochem. Bioenerg.* **1993**, *31*, 65.

(5) Cunnane, V. J.; Schiffrin, D. J.; Beltran, C.; Geblewicz, G.; Solomon, T. *J. Electroanal. Chem.* **1988**, *247*, 203.
(6) Koryta, J.; Skalicky, M. *J. Electroanal. Chem.* **1987**, *229*, 265.
(7) Kharkats, Y. I.; Samek, Z.; Gurevich, Y. Y. *J. Electroanal. Chem.* **1986**, *204*, 257.
(8) Gurevich, Y. Y.; Kharkats, Y. I. *J. Electroanal. Chem.* **1986**, *200*, 3.
(9) Schmickler, W. *J. Electroanal. Chem.* **1997**, *426*, 5.
(10) Hanna, G. J.; Noble, R. D. *Chem. Rev.* **1985**, *85*, 583.
(11) Cheng, Y.; Schiffrin, D. *J. Electroanal. Chem.* **1996**, *409*, 9.
(12) Cheng, Y.; Schiffrin, D. *J. Electroanal. Chem.* **1997**, *429*, 37.
(13) Berendsen, H. J. C.; Grigera, J. R.; Straatsma, T. P. *J. Phys. Chem.* **1987**, *91*, 6269.
(14) Brooks, B. B.; Bruccolery, R. E.; Olafson, B. D.; States, D. J.; Swaminathan, S.; Karplus, M. J. *J. Comput. Chem.* **1983**, *4*, 187.
(15) Jorgensen, W. L.; Tirado-Rives, J. *J. Am. Chem. Soc.* **1988**, *110*, 1657.
(16) Frisch, M. J.; Trucks, G. W.; Schlegel, H. B.; Gill, P. M. W.; Johnson, B. G.; Robb, M. A.; Cheeseman, J. R.; Keith, T.; Petersson, G. A.; Montgomery, J. A.; Raghavachari, K.; Al-Laham, M. A.; Zakrzewski, V. G.; Ortiz, J. V.; Foresman, J. B.; Cioslowski, J.; Stefanov, B. B.; Nanayakkara, A.; Challacombe, M.; Peng, C. Y.; Ayala, P. Y.; Chen, W.; Wong, M. W.; Andres, J. L.; Replogle, E. S.; Gomperts, R.; Martin, R. L.; Fox, D. J.; Binkley, J. S.; Defrees, D. J.; Baker, J.; Stewart, J. P.; Head-Gordon, M.; Gonzalez, C.; Pople, J. A. *Gaussian 94, Revision D.4*; Gaussian, Inc.: Pittsburgh, PA, 1995.
(17) Bayly, C. I.; Cieplak, P.; Cornell, W. D.; Kollman, P. A. *J. Phys. Chem.* **1993**, *97*, 10269.
(18) Forrester, T. W.; Smith, W. *DLPOLY (2.1 version)*; CCLRC: Daresbury Laboratory, 1995.
(19) Hoover, W. G. *Phys. Rev.* **1985**, *A31*, 1695.
(20) Melchionna, S.; Ciccotti, G.; Holian, B. L. *Mol. Phys.* **1993**, *78*, 533.
(21) Forrester, T. W.; Smith, W. *Mol. Simulation* **1994**, *13*, 195.
(22) Jorgensen, W. L.; Tirado-Rives, J. *J. Am. Chem. Soc.* **1984**, *106*, 6638.
(23) *Handbook of Chemistry and Physics*; Weast, R. C., Ed.; CRC Press: Boca Raton, FL, 1989.